RESEARCH ARTICLE | JUNE 14 2023

Electrostatic upper-hybrid mode instability driven by a ring electron distribution \odot

Peter H. Yoon 🕶 📵 ; Yoshiharu Omura 📵



Physics of Plasmas 30, 062107 (2023) https://doi.org/10.1063/5.0151710





CrossMark





Electrostatic upper-hybrid mode instability driven by a ring electron distribution

Cite as: Phys. Plasmas **30**, 062107 (2023); doi: 10.1063/5.0151710 Submitted: 24 March 2023 · Accepted: 26 May 2023 · Published Online: 14 June 2023













AFFILIATIONS

- 1 Institute for Physical Science and Technology (IPST), University of Maryland, College Park, Maryland 20742, USA
- ²Research Institute for Sustainable Humanosphere (RISH), Kyoto University, Gokasho, Uji, Kyoto 611-0011, Japan

ABSTRACT

Quasi electrostatic fluctuations in the upper-hybrid frequency range are commonly detected in the planetary magnetospheric environment. The origin of such phenomena may relate to the instability driven by a loss-cone feature associated with the electrons populating the dipole-like magnetic field. The present paper carries out a one-dimensional electrostatic particle-in-cell simulation accompanied by a reduced quasilinear kinetic theoretical analysis to investigate the dynamics of the upper-hybrid mode instability driven by an initial ring electron distribution function, which is a form of loss-cone distribution. A favorable comparison is found between the two approaches, which shows that the reduced quasilinear theory, which is grounded in the concept of a model of the particle distribution function that is assumed to maintain a fixed mathematical form except that the macroscopic parameters that define the distribution are allowed to evolve in time, can be an effective tool in the study of plasma instabilities, especially if it is guided by and validated against the more rigorous simulation result.

Published under an exclusive license by AIP Publishing. https://doi.org/10.1063/5.0151710

I. INTRODUCTION

Planetary magnetosphere is replete with quasi-electrostatic fluctuations in the upper-hybrid frequency range. Earth's magnetosphere, including the radiation belt and the ring current region, shows that such high-frequency fluctuations are pervasively detected during the quiet time condition. 1-8 These fluctuations are sometimes accompanied by emissions in the multiple harmonic electron cyclotron frequencies, which are interpreted as Bernstein modes.9 In addition to the magnetospheric examples, early laboratory experiments as well as certain type of solar radio emissions have been interpreted in terms of the Bernstein modes and related instabilities. 10-20 The fluctuations in the upper-hybrid frequency range, especially if they are accompanied by multiple-harmonic cyclotron emissions, naturally lend themselves to theoretical interpretation based upon the notion of spontaneous emission in magnetized plasmas.^{21–31} This is because in thermal plasmas, fluctuations ranging from all frequencies and wave numbers are spontaneously emitted, which includes plasma eigenmodes and noneigenmodes, although the emissions are enhanced in the vicinity of eigenmodes. As such, multiple-harmonic Bernstein modes are all spontaneously emitted in thermal plasmas.

On the other hand, fluctuations with peak intensity located in the close vicinity of upper-hybrid frequency may be associated with the collective mode excitation, that is, instability. This is because the

instability is dictated by resonant wave-particle interaction, which when coupled with the unstable feature associated with the electron distribution, places limitations on the frequency range of the wave excitation. For instance, let us consider the weakly-relativistic cyclotron resonance condition for perpendicular propagation, $\gamma \omega - n\Omega_e \approx [1 + v^2/(2c^2)]\omega$ $-n\Omega_e = 0$, where ω is the wave angular frequency, $\Omega_e = eB_0/m_e c$ is the electron cyclotron frequency, with e, B_0 , m_e , and c being the unit electric charge, ambient magnetic field intensity, the electron rest mass, and the speed of light *in vacuo*, and *n* is an integer. Then, the resonance condition is given by $v^2 = 2c^2(n\Omega_e/\omega - 1)$. This represents a circle in velocity space, provided $\omega < n\Omega_e$. Suppose also that the free energy source for the instability resides with the inverted population in perpendicular velocity space, $\partial f/\partial v_{\perp} > 0$, over a certain range of perpendicular velocity space, where f represents the electron velocity space distribution function. The resonance circle and the range of velocity space over which $\partial f/\partial v_{\perp} > 0$ takes place must be matched for the wave excitation, and since not all possible n satisfies such a favorable condition, the wave emission will necessarily be restricted to a narrow range. Energetic electrons populating the magnetosphere are subject to the field-aligned inhomogeneity, as they travel back and forth along the dipole-like magnetic field. Consequently, the natural state of the velocity distribution function may contain the loss-cone feature, which is a consequence of the

a) Author to whom correspondence should be addressed: yoonp@umd.edu

magnetic mirror effect. Such a loss-cone distribution naturally provides the condition for an instability.

The ring distribution function is a form of loss-cone distribution. It is known that the ring or more generally, the loss-cone distribution, is unstable to the excitation of upper-hybrid mode instability. $^{10,12-18,20,32-38}$ However, linear theory is limited in that it cannot predict the nonlinear state of the instability. Consequently, to understand the nonlinear behavior, numerical simulations of instabilities excited in a plasma with thermal ring electron distribution have been carried out.³⁹⁻⁵⁰ These include particle-in-cell (PIC) or Vlasov simulations performed under the assumption of one- or two-dimensional systems, with electrostatic or electromagnetic formalism, and for uniform as well as for inhomogeneous medium. However, in the simplifying limit of electrostatic upper-hybrid mode instability propagating in exactly perpendicular direction with respect to the ambient magnetic field, it is possible to carry out a quasilinear kinetic theoretical analysis in addition to the linear theoretical calculation, which can be compared against the PIC simulation. Indeed, Ref. 53 performed such an analysis, where the linear theory of upper-hybrid mode instability is worked out under the assumption of an initial Dory-Guest-Harris (DGH) model distribution³⁵ for energetic but tenuous electrons. Reference 53 also formulated a quasilinear theory and made a direct comparison against one-dimensional (1D) PIC simulation.

The purpose of this paper is to revisit Ref. 53. The type of quasilinear theory employed in Ref. 53 is a reduced theory in that, instead of directly solving for the velocity-space diffusion equation, the mathematical form of distribution function is assumed to be invariant except that the underlying parameters are allowed to change in time. This type of forced self-similar quasilinear theory has been used extensively for bi-Maxwellian distributions of electrons, protons, and alphaparticles, with applications in the context of the solar wind research. 54-63 Upon comparisons with PIC code simulations, the bi-Maxwellian based reduced quasilinear theory was found to be in reasonable agreement. Reference 53 attempted to apply the similar scheme to the DGH model and the ensuing Bernstein mode instability. However, the DGH model adopted in Ref. 53 turned out to be somewhat restrictive in that the comparison with the simulation revealed only a qualitative convergence.

In the DGH model, the loss-cone feature is implemented by multiplying a polynomial velocity factor to the Maxwellian perpendicular distribution, $f_{\rm DGH} \propto v_{\perp}^{2l} \exp{(-m_e v_{\perp}^2/2T)}$, where T denotes the velocity dispersion (or "temperature"). In the DGH model, the index $l = 0, 1, 2, \dots$ represents discrete positive integers, which are not smoothly varying. As such, the continuous time variation of ring speed is difficult to model within the context of DGH distribution. For this reason, Ref. 53 only allowed the thermal spread to vary in time while considering the l value as fixed. To address this shortcoming, we revisit the same problem by adopting the ring model instead, $f_{\rm ring} \propto \exp\left[-m_e(v_{\perp}-v_0)^2/2T\right]$, for which, both the ring speed v_0 and the perpendicular "temperature" associated with the ring distribution, T, can be treated as smoothly-varying functions of time. In order to accurately model the dynamics of upper-hybrid instability and its feedback on the ring distribution, we first carry out the 1D electrostatic (ES) PIC simulation, which will be used as a guide for theoretical modeling of quasilinear dynamics. The PIC code is the standard KEMPO, originally developed by one of the present authors.⁶⁴ In the remainder of this paper, we systematically discuss the present findings.

The organization of the present paper is as follows: In Sec. II, we discuss the linear theory of upper-hybrid/Bernstein mode instability. Section III discusses the 1D ES PIC code simulation, whose outcome provides the guideline for the subsequent quasilinear modeling, which is presented in Sec. IV. Section V summarizes and concludes the present paper and also discusses the ramification of the present paper.

II. UPPER-HYBRID MODE INSTABILITY DRIVEN BY A RING ELECTRON DISTRIBUTION

In the present analysis, we assume that all perturbations propagate in a direction exactly perpendicular to the ambient magnetic field. We also assume that electrostatic interaction is dominant. Under non-relativistic treatment, resonant wave-particle interaction is absent for perpendicular propagation. We assume (weakly) relativistic formalism in the growth rate calculation. The protons are treated as a neutralizing background. An isotropic Maxwellian core electrons support the waves, while tenuous but energetic electrons possessing a ring feature excite the instability. In the computation of the dispersion relation, we resort to the non-relativistic formalism. The weakly relativistic correction to the wave-particle resonance condition is implemented only in the growth rate expression. We resort to the (weakly) relativistic wave-particle resonance condition because the non-relativistic formalism does not lead to the resonant instability. Thus, the real frequency is determined from the nonrelativistic dispersion relation,

$$0 = 1 + \frac{\omega_{pe}^2}{k_{\perp}^2} \sum_{n=-\infty}^{\infty} \frac{n\Omega_e}{\omega - n\Omega_e} \int d\mathbf{v} \frac{J_n^2(b_{\perp})}{v_{\perp}} \frac{\partial f_0}{\partial v_{\perp}}, \tag{1}$$

where $\omega_{pe}=(4\pi n_0 e^2/m)^{1/2}$ is the plasma frequency, $b_\perp=k_\perp v_\perp/\Omega_e$, and $f_0(\mathbf{v})=(2\pi\alpha_0^2)^{-3/2}$ exp $[-v^2/(2\alpha_0^2)]$ represents the thermal background electron velocity distribution function. Here, n_0 denotes the ambient plasma density, and I_n stands for the Bessel function of the first kind of order n. The background electron thermal speed is defined by $\alpha_0=T_0/m_e$, where T_0 designates the electron temperature (given in terms of the unit of energy, hence, Boltzmann constant is absent). Making use of the background distribution f_0 and carrying out the velocity integral, one obtains the familiar dispersion relation that supports the Bernstein waves, $^{9.32}$

$$0 = \epsilon_r(k_\perp, \omega_r) = 1 + \frac{\omega_{pe}^2}{\Omega_e^2 \lambda} \left(1 - \Lambda_0(\lambda) - \sum_{n=1}^{\infty} \frac{2\omega_r^2 \Lambda_n(\lambda)}{\omega_r^2 - n^2 \Omega_e^2} \right), \quad (2)$$

where $\lambda = k_{\perp}^2 \alpha_0^2 / \Omega_e^2$, $\Lambda_n(\lambda) = I_n(\lambda) e^{-\lambda}$, and $I_n(\lambda)$ represents the modified Bessel function of the first kind of order n.

As noted, in computing for the real frequency ω_r via Eq. (2), we do not consider the relativistic effects, but in the growth rate expression, ω_i (imaginary part of the complex frequency), we retain the weakly relativistic effects in the resonance condition, ¹⁶

$$\omega_{i} = \frac{n_{h}}{n_{0}} \frac{\pi \omega_{pe}^{2}}{R k_{\perp}^{2}} \int d\mathbf{v} \sum_{n=-\infty}^{\infty} J_{n}^{2} \left(\frac{k_{\perp} v_{\perp}}{\Omega_{e}}\right) \delta\left(\frac{v^{2}}{2c^{2}} - \frac{n\Omega_{e} - \omega_{r}}{\omega_{r}}\right) \frac{1}{v_{\perp}} \frac{\partial f_{h}}{\partial v_{\perp}},$$

$$R = \frac{\partial \epsilon_{r}(k_{\perp}, \omega_{r})}{\partial \omega_{r}} = \sum_{n=1}^{\infty} \frac{4n^{2} \Lambda_{n}(\lambda)}{\lambda} \frac{\omega_{r} \omega_{pe}^{2}}{(\omega_{r}^{2} - n^{2} \Omega_{e}^{2})^{2}},$$
(3)

where n_h denotes the "hot" electron density, whose velocity distribution function f_h is given by the "ring" model,

$$f_{h} = \frac{1}{(2\pi)^{3/2} A_{0} \alpha_{\perp}^{2} \alpha_{\parallel}} \exp\left(-\frac{(v_{\perp} - v_{0})^{2}}{2\alpha_{\perp}^{2}} - \frac{v_{\parallel}^{2}}{2\alpha_{\parallel}^{2}}\right),$$

$$A_{0} = 2 \int_{0}^{\infty} dx x \exp\left[-\left(x - \frac{v_{0}}{\sqrt{2}\alpha_{\perp}}\right)^{2}\right].$$
(4)

Note that the normalization constant A_0 can further be manipulated in terms of the error function, specifically $A_0 = \exp(-x_0^2) + x_0\sqrt{\pi}[1$ +erf (x_0)], where $x_0 = v_0/\sqrt{2}\alpha_{\perp}$ and erf(x) is the error function, but in the later numerical growth rate computation we encounter a class of similar x integrals, which we choose to evaluate numerically. Thus, for the sake of numerical consistency, we retain the integral form of A_0 . Note also that, without the relativistic correction (that is, if we let $v^2/c^2 \rightarrow 0$), the resonant delta function condition does not involve the velocity; hence, the problem becomes ill-defined. This shows that for non-relativistic Bernstein mode instabilities driven by a ring electron distribution one cannot approach the problem from the perspective of resonant instability. Instead, the non-relativistic Bernstein mode instability requires the formulation that takes into account of the complex angular frequency ω such that both the real and imaginary parts of ω are to be solved from the transcendental dispersion relation. In fact, an early Ref. 11 has considered just such an instability by taking the electron distribution function to have a delta-function ring feature, $f_e(v_\perp) \propto \delta(v_\perp - v_{\perp 0})$, and demonstrated that the reactive type of Bernstein mode instability takes place when the two adjacent cyclotron harmonic modes merge to form a complex conjugate pair. Recently, Refs. 45 and 46 have numerically simulated such an instability. One final note before moving on relates to an early Ref. 16, who also discussed the relativistic effect associated with the resonant Bernstein mode instability. While in the present discussion we restrict ourselves to the strictly perpendicular propagation and have approximated the Lorentz factor by $\gamma \approx 1 + v^2/2c^2$, under the weakly relativistic approximation, Ref. 16 considered an arbitrary angle of propagation, including finite k_{\parallel} . However, they note that for small k_{\parallel} , the cyclotron resonance condition amounts to a circle in momentum space, which is equivalent to the present situation.

Upon inserting the hot ring distribution f_h to the growth rate expression, after some manipulations that include the use of delta function resonance condition to eliminate the v_{\parallel} integral, one arrives at

$$\omega_{i} = -\frac{n_{h}}{n_{0}} \frac{2\pi^{1/2}}{A_{0}R} \frac{\omega_{pe}^{2}}{k_{\perp}^{2}} \frac{c^{2}}{\alpha_{\perp}^{3}} \alpha_{\parallel} \sum_{n=1}^{\infty} \Theta(n\Omega_{e} - \omega_{r})
\times \int_{0}^{x_{*}} dx \frac{(x - x_{0})J_{n}^{2}(bx)}{\sqrt{x_{*}^{2} - x^{2}}}
\times \exp\left[-(x - x_{0})^{2} - \frac{\alpha_{\perp}^{2}}{\alpha_{\parallel}^{2}} (x_{*}^{2} - x^{2})\right],$$

$$x_{*}^{2} = \frac{c^{2}}{\alpha_{\perp}^{2}} \frac{n\Omega_{e} - \omega_{r}}{\omega_{r}}, \quad x_{0} = \frac{v_{0}}{\sqrt{2}\alpha_{\perp}}, \quad b = \frac{\sqrt{2}k_{\perp}\alpha_{\perp}}{\Omega_{e}},$$
(5)

where $\Theta(x)$ is the Heaviside step function, $\Theta(x) = 1$ for x > 0, and zero otherwise.

In the present study, we consider the following input parameters:

$$\frac{\alpha_0}{c} = 0.025 = \frac{\alpha_{\perp}}{c} = \frac{\alpha_{\parallel}}{c}, \quad \frac{v_0}{\alpha_0} = 10, \quad \frac{\omega_{pe}}{\Omega_e} = 10, \quad \frac{n_h}{n_0} = \frac{4}{104}.$$
 (6)

Figure 1 plots the normalized real frequency ω_r/Ω_e (in red) and normalized growth rate ω_i/Ω_e [×4] — that is, the growth rate multiplied by a factor of four — vs normalized wave number $k_{\perp}\alpha_0/\Omega_e$. We have solved the cyclotron harmonics up to n = 20, and computed the growth rate for each mode. In plotting the growth rate for each harmonic, we upshifted the vertical position for each harmonic mode growth rate according to the corresponding real frequency so that the real frequency and its growth rate can easily be paired with. Note that we have numbered the harmonic modes, n = 1, 2, 3, etc. When the growth rate turns negative (damping) we do not plot its value to avoid cluttering. Hence, we only plot the positive part of ω_i . This procedure aids the visualization, but in the subsequent quasilinear wave analysis, we allow each harmonic mode to freely absorb the wave energy when ω_i becomes negative. As Fig. 1 indicates, the highest growth takes place at n = 10 harmonic, which corresponds to the upper-hybrid frequency range. The next higher mode, n = 11, also has some growth rate associated with it, as do all lower harmonics, $n \leq 9$, albeit, their growth rates are extremely low when compared with the leading mode n = 10. We found that all modes higher than n = 12 are stable.

We have formulated a reduced quasilinear kinetic theory to investigate the dynamics of upper-hybrid instability beyond linear stage. The method involves making an assumption about the mathematical form of the hot electron distribution as a function of time. At t=0, the hot electrons are, of course, distributed according to the ring model, (4), but subsequent time evolution is difficult to predict *a priori*. In general, we expect that the positive gradient along v_{\perp} direction, which provides the free energy source for the instability, will be

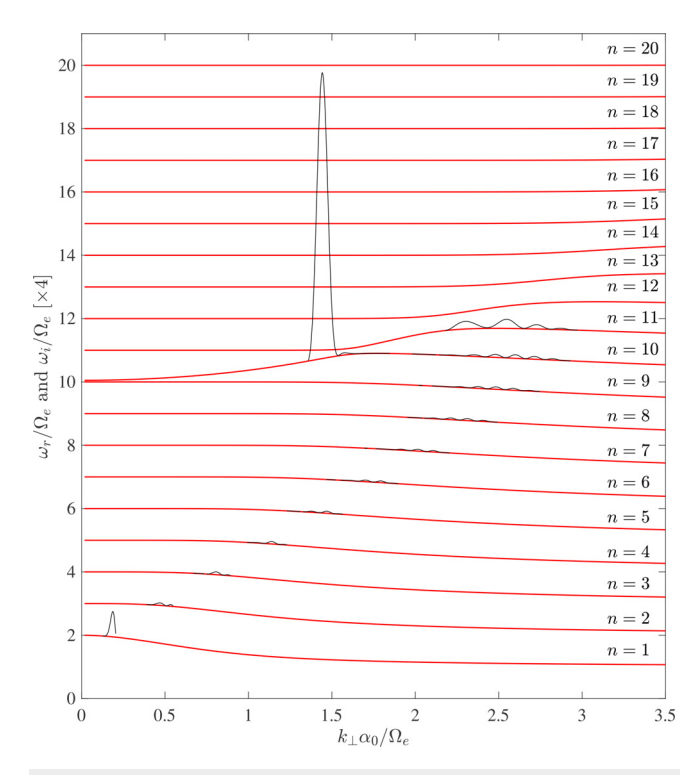


FIG. 1. The real frequency (dispersion relation) plotted in red, and growth rate for each harmonic (multiplied by a factor of 4 and upshifted vertically by adding the corresponding real frequency), vs the normalized wave number.

diminished as the instability is excited, but the precise details of how such a process will take place is non-trivial. This contrasts with transverse instabilities excited in a bi-Maxwellian plasma. For transverse modes involving the cyclotron resonance condition, the dominant effect is known to be the pitch-angle diffusion, which generally preserves the bi-Maxwellian nature of the underlying plasma distribution. As such, the assumption of bi-Maxwellian form of particle distribution for all times is generally proven to be quite accurate when compared against the simulations. 54-63 However, for the ring, or more generally, the loss-cone distribution, the situation is more subtle. In an earlier work,⁵³ we assumed that the initial form of DGH model, $f_h \propto v_\perp^{2l} \exp{(-m_e v_\perp^2/2T_\perp)}$ remained invariant except that T_\perp was allowed to changeover time. Under such an assumption, the ring speed is forced to remain largely invariant but only the velocity spread in v_{\perp} direction is allowed to increase in time. However, as already noted, such an approach did not produce a completely satisfactory comparison. In order to aid the theoretical modeling, we, thus, turn to the PIC simulation, which is discussed next. As it will be shown, the PIC simulation indicates that not only the thermal spread increases in time, but also, the ring speed undergoes a gradual reduction as the instability is excited and saturated. Thus, the theoretical modeling of the time-dependent distribution will be guided by such a result. Before we discuss the details of reduced quasilinear theory, let us discuss the simulation result.

III. SIMULATION OF UPPER-HYBRID MODE INSTABILITY

The present simulation is based on KEMPO code.⁶⁴ As the theory assumes 1D electrostatic (ES) situation, we also implement the 1D ES version of the KEMPO code (although the code is available in 2D as well as in EM versions). In this code, we use periodic boundary conditions for all physical quantities. Particles are advanced in time by the Boris algorithm, and the electrostatic field is calculated from the Poisson equation. The charge density and electric field are weighed to and from the grid by a linear first order weighting method. The ambient magnetic field lies perpendicular to the simulation axis.

Figure 2 displays the wave energy density vs time computed from the simulation. It is seen that the electrostatic wave energy density grows from the initial noise level rather rapidly, within a short time span of $\Omega_e t \sim 0.2$, until it reaches a plateau, and subsequently, the intensity steadily rises until it reach a maximum value around $\Omega_e t \sim 10$, beyond which, the wave energy slowly decays until the end of the simulation run. One may check that the initial growth rate is consistent with the theory. The highest growth rate associated with n = 10 mode around $k_{\perp}\alpha_0/\Omega_e \approx 1.5$, shown in Fig. 1, turns out to be $\gamma_{
m max}/\Omega_e\sim 2.25$ or so. If we take the initial level of electrostatic wave energy to be $I_0 \sim 1 \times 10^{-1}$ or so, then according to Fig. 2 we find, upon a visual inspection, that the intensity has amplified to $I \sim 3 \times 10^{-1}$ within a short time span of $\Omega_e t \sim 0.2$. From this, it is a simple math to see that $\ln(I/I_0) \sim \mathcal{O}(1)$ or so, which is roughly in agreement with the exponential growth factor $2\gamma_{\max}\Delta t\sim \mathcal{O}(0.9)$, if we choose $\Delta t \sim 0.2$. The gradual reduction of the wave energy beyond the peak intensity can be interpreted as the result of electrons slowly reabsorbing the wave energy. Later, we will take the snapshots of electron distribution function at intervals corresponding to $\Omega_e t = 6$, which represents the growth phase of wave intensity; to $\Omega_e t = 10$,

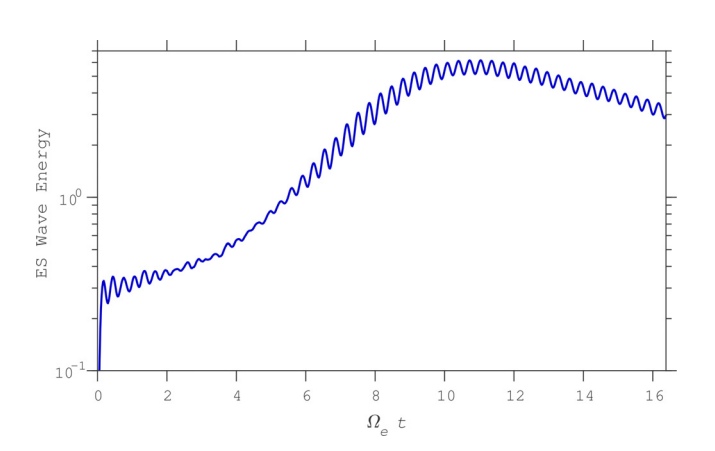


FIG. 2. Electrostatic wave energy density vs time. The normalization is arbitrary. It is seen that the wave energy density exponentially grows from its initial noise, saturates, and undergoes gradual reduction in intensity beyond the saturation stage.

which is at the point when the wave intensity reaches its peak; to $\Omega_e t = 16$, which is close to the end of the simulation shown in Fig. 2; and to $\Omega_e t = 20$.

In Fig. 3, we display the dynamic spectrum of wave energy density as a function of wave number and time. It is seen that the highest wave growth takes place slightly below $k_{\perp}\alpha_0/\Omega_e\sim 1.5$ or so, but some adjacent modes are also seen to have weak wave intensities. The mode corresponding to $k_{\perp}\alpha_0/\Omega_e\sim 1.5$ is associated with the upperhybrid frequency, which can be confirmed upon comparison with the theoretical dispersion relation shown in Fig. 1, but we must also emphasize that the agreement is somewhat qualitative rather than exact, since the theory predicts $k_{\perp}\alpha_0/\Omega_e\sim 1.5$ while the simulation shows somewhat broader range, with the peak around $k_{\perp}\alpha_0/\Omega_e\sim 1.25$ at $\Omega_e t\sim 10$, but shifting more close to $k_{\perp}\alpha_0/\Omega_e\sim 1.5$ at later times. The exact cause of such a minor discrepancy is not known at

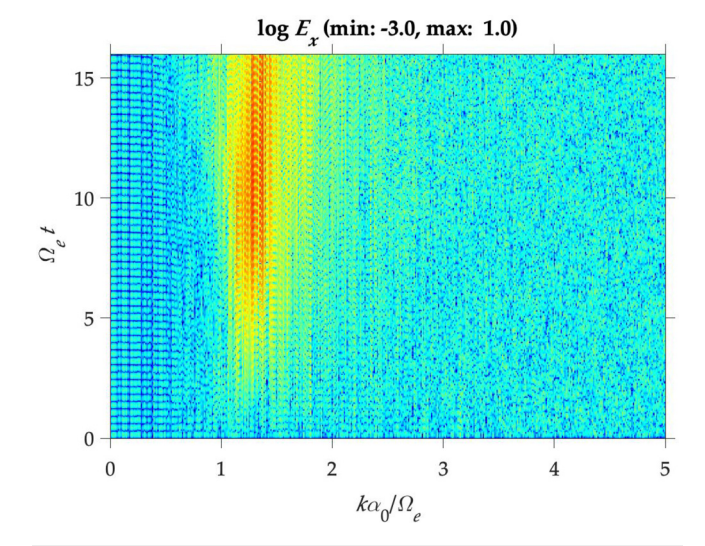


FIG. 3. Dynamic spectrum showing the wave spectrum in k space evolving over time. Note that the highest wave growth takes place around $k_{\perp}\alpha_0/\Omega_{\rm e}\sim$ 1.5 or so, with some adjacent modes also showing weak wave intensities.

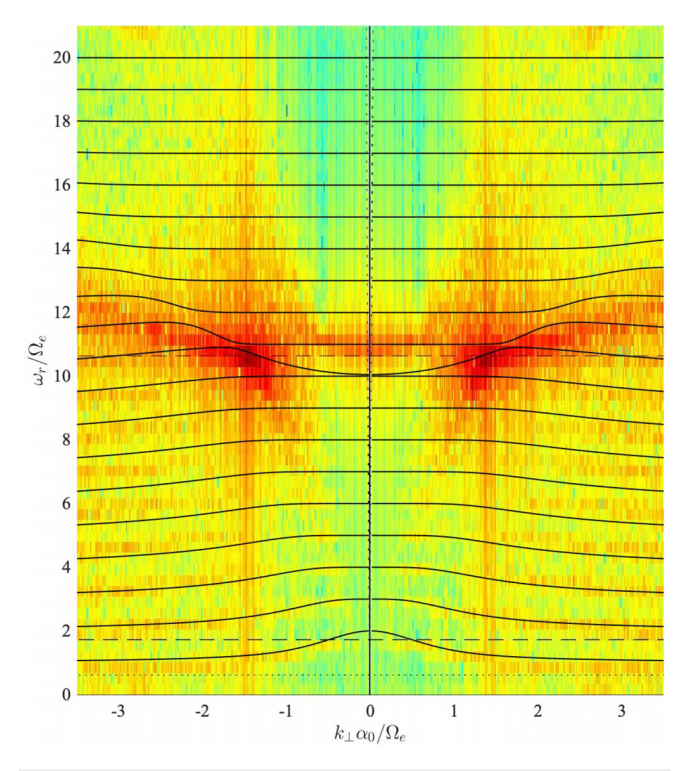


FIG. 4. Simulated frequency-wave number spectrum and theoretical dispersion relation superposed on top of the simulated spectrum.

this time, but this could be related to some unspecified nonlinear effects. We note that the time period centered around $\Omega_e t \sim 10$ is already beyond the linear growth stage. We also note that the simulated dynamic spectrum features a broad range of low-intensity noise-like background. Such a signature might indicate certain nonlinear processes, or perhaps, they indicate the weak growths associated with multiple harmonic modes as shown in Fig. 1—recall that according to Fig. 1, all harmonics lower than n=11 have some weak growth rates.

To further confirm that the peak intensity near $k_{\perp}\alpha_0/\Omega_e\sim 1.5$ is indeed the upper-hybrid mode, or n=10 mode, as following the convention in Fig. 1, we plot in Fig. 4, the simulated frequency-wave number spectrum. We have also superposed the theoretical dispersion relation on top of the simulated spectrum. As one may appreciate, the peak wave growth coincides with the upper-hybrid mode which, according to the linear theory, has the highest initial growth rate. This confirms that the simulation result is consistent with the linear theoretical prediction.

Our purpose is not simply to confirm the linear theory by PIC simulation but also to formulate an efficient quasilinear theory by modeling a time-dependent particle distribution function. For this goal, the snapshot of electron distribution function at selected intervals would serve the purpose. Thus, in Fig. 5, we plot the perpendicular electron velocity distribution function at four different intervals indicated in Fig. 2. These are, as noted already, $\Omega_e t = 6$ (the wave growth phase), $\Omega_e t = 10$ (quasi saturation phase when the wave intensity has reached its peak), and $\Omega_e t = 16$ (near the end of the simulation run), and one last stage at $\Omega_e t = 20$. For each panel, we also plot the initial ring distribution to facilitate the visual comparison. From Fig. 5, one may discern that the temporal evolution of the perpendicular velocity

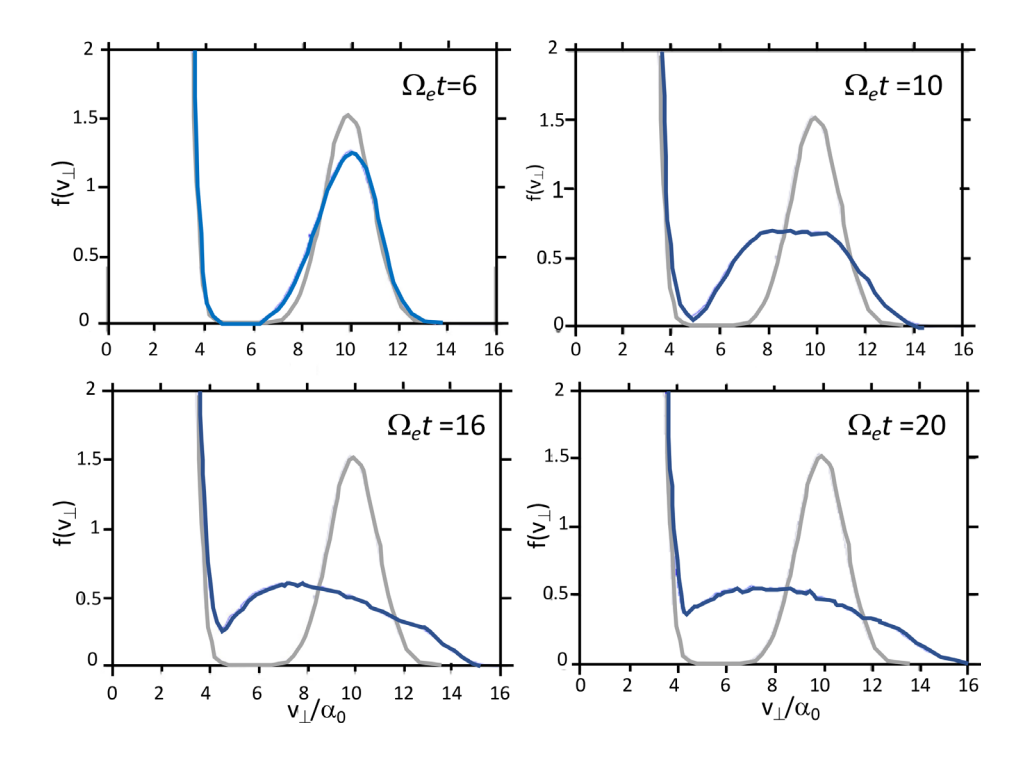


FIG. 5. Snapshots of perpendicular electron velocity distribution function at three four intervals indicated in the text, namely, $\Omega_{\rm e}t=6$, 10, 16, and 20.

distribution function involves concomitant reduction of the ring speed v_0 as well as an increase in thermal spread α_\perp . With such useful pieces of information, we next formulate a reduced quasilinear kinetic theory. As mentioned earlier, with the DGH model adopted in Ref. 53, the reduction of ring speed is difficult to model, as the effective ring speed in the DGH model is fixed by the term v_\perp^{2l} , with integer l. For this reason, Ref. 53 only modeled the increasing thermal spread feature associated with the DGH model. In contrast, the present ring model is more flexible in this regard. The dynamical progression of the ring speed v_0 and perpendicular thermal spread α_\perp will be determined from the quasilinear theory, which is discussed next. One final comment before moving on is that the present PIC simulation shows that parallel velocity distribution function remains largely invariant (the plot of parallel velocity distribution is not shown). As it will be shown, this is consistent with the quasilinear theory.

IV. QUASILINEAR KINETIC THEORY FOR TIME-DEPENDENT RING DISTRIBUTION

In formulating and solving for the quasilinear kinetic theory, we assume that the hot electron distribution function is given by the same mathematical form as specified in Eq. (4), except that v_0 and α_{\perp} evolve in time. This model is guided by the simulation result, which is discussed in relation to Fig. 5. The precise description of how these two quantities evolve is dictated by the quasilinear kinetic theory. The particle kinetic equation that governs the time evolution of hot electron distribution function, under the approximation of weakly relativistic wave-particle resonance, and for exactly perpendicular propagation of electrostatic modes, is given by $^{51-53}$

$$\frac{\partial f_h}{\partial t} = \frac{2\pi^2 e^2}{m_e^2} \sum_{n=-\infty}^{\infty} \int_0^{\infty} \frac{dk_{\perp} k_{\perp}}{\omega_r} \frac{n\Omega_e}{v_{\perp}} \frac{\partial}{\partial v_{\perp}} J_n^2 \left(\frac{k_{\perp} v_{\perp}}{\Omega_e}\right) W(k_{\perp}) \delta
\times \left(\frac{v^2}{2c^2} - \frac{n\Omega_e - \omega_r}{\omega_r}\right) \frac{n\Omega_e}{v_{\perp}} \frac{\partial f_h}{\partial v_{\perp}}.$$
(7)

Here, $W(k_\perp)$ represents the spectral wave energy density for the electrostatic mode, which satisfies the wave kinetic equation. The quantity $W(k_\perp)$ is a combination of individual harmonic modes, $W(k_\perp) = \sum_{n=-\infty}^{\infty} W_n(k_\perp)$, with each harmonic component satisfying the wave equation, $\partial W_n(k_\perp)/\partial t = 2\omega_i^n(k_\perp)W_n(k_\perp)$, where $\omega_i^n(k_\perp)$ denotes the n-th harmonic mode growth rate—see Fig. 1. Note that Ref. 52 considered a similar problem as compared to the present paper in that Ref. 52 employed the quasilinear theory to analyze the upperhybrid mode instability, but unlike our approach (to be discussed below) the author of Ref. 52 sought an analytical solution to the diffusion equation by considering an approximate form of Bessel function.

It is straightforward to show that the parallel temperature is invariant, which can be seen by taking the second parallel velocity moment of Eq. (7),

$$\int d\mathbf{v} \, v_{\parallel}^2 \, \frac{\partial f_h}{\partial t} = 0. \tag{8}$$

Consequently, the parallel thermal spread α_{\parallel} should remain constant in time. This conforms with PIC simulation, which we have already discussed.

In what follows, we assume that f_h is given by the form (4) but v_0 and α_{\perp} evolve in time. This model is guided by the simulated perpendicular velocity distribution function shown in Fig. 5, and such a

model also differs from the assumed time-dependent DGH model considered in Ref. 53, where only the thermal spread was allowed change in time. For the purpose of deriving the evolution equations for v_0 and α_{\perp} , it is sufficient to consider the first and second perpendicular velocity moments of Eq. (7),

$$\frac{\partial}{\partial t} \int d\mathbf{v} \begin{pmatrix} v_{\perp} \\ v_{\perp}^{2} \end{pmatrix} f_{h} = -\frac{2\pi^{2}e^{2}}{m_{e}^{2}} \sum_{n=-\infty}^{\infty} n^{2} \Omega_{e}^{2} \int_{0}^{\infty} \frac{dk_{\perp}k_{\perp}}{\omega_{r}} W(k_{\perp})
\times \int d\mathbf{v} J_{n}^{2} \left(\frac{k_{\perp}v_{\perp}}{\Omega_{e}}\right) \begin{pmatrix} 1 \\ 2v_{\perp} \end{pmatrix}
\times \delta \left(\frac{v^{2}}{2c^{2}} - \frac{n\Omega_{e} - \omega_{r}}{n\Omega}\right) \frac{1}{v_{\perp}^{2}} \frac{\partial f_{h}}{\partial v_{\perp}}.$$
(9)

The left-hand side of Eq. (9) can be evaluated as follows upon making an explicit use of model distribution (4),

$$\frac{\partial}{\partial t} \int d\mathbf{v} v_{\perp} f_{h} = \left(\frac{A_{1}}{A_{0}} - x_{0} \frac{A_{0} A_{2} - A_{1}^{2}}{A_{0}^{2}} \right) \frac{d\alpha_{\perp}}{dt} + \frac{\sqrt{2} (A_{0} A_{2} - A_{1}^{2})}{A_{0}^{2}} \frac{dv_{0}}{dt},$$

$$\frac{\partial}{\partial t} \int d\mathbf{v} v_{\perp}^{2} f_{h} = \alpha_{\perp} \left[\left(\frac{2A_{2}}{A_{0}} - x_{0} \frac{A_{0} A_{3} - A_{1} A_{2}}{A_{0}^{2}} \right) \frac{d\alpha_{\perp}}{dt} + \frac{\sqrt{2} (A_{0} A_{3} - A_{1} A_{2})}{A_{0}^{2}} \frac{dv_{0}}{dt} \right],$$

$$+ \frac{\sqrt{2} (A_{0} A_{3} - A_{1} A_{2})}{A_{0}^{2}} \frac{dv_{0}}{dt},$$

$$A_{n} = 2 \int_{0}^{\infty} dx x^{n+1} \exp\left[-(x - x_{0})^{2} \right], \quad x_{0} = \frac{v_{0}}{\sqrt{2}\alpha_{\perp}}.$$
(10)

The right-hand side of Eq. (9) can be evaluated in the same manner as in the derivation of growth rate (5). Upon carrying out the detailed manipulations and rearranging the resultant expressions, we arrive at the following dynamic equations for the two quantities v_0 and α_\perp ,

$$\frac{dv_0}{dt} = \frac{\mathcal{N}_1}{\mathscr{D}} \Gamma_1 - \frac{\mathcal{N}_2}{\mathscr{D}} \Gamma_2, \quad \frac{d\alpha_\perp}{dt} = -\frac{\mathcal{M}_1}{\mathscr{D}} \Gamma_1 + \frac{\mathcal{M}_2}{\mathscr{D}} \Gamma_2,
\mathcal{N}_1 = \sqrt{2}A_0A_2 - (A_0A_3 - A_1A_2) \frac{v_0}{\alpha_\perp},
\mathcal{N}_2 = A_0A_1 - \sqrt{2}(A_0A_2 - A_1^2) \frac{v_0}{\alpha_\perp},
\mathcal{M}_1 = A_0A_3 - A_1A_2, \quad \mathcal{M}_2 = \sqrt{2}(A_0A_2 - A_1^2),
\mathcal{D}_1 = 2A_1A_2^2 - A_1(A_0A_3 + A_1A_2).$$
(11)

where

$$\begin{pmatrix}
\Gamma_{1} \\
\Gamma_{2}
\end{pmatrix} = \frac{8\pi^{3/2}e^{2}c^{2}}{m_{e}^{2}\alpha_{\perp}^{2}} \int_{0}^{\infty} \frac{dk_{\perp}k_{\perp}}{\omega_{r}} W(k_{\perp})$$

$$\times \sum_{n=1}^{\infty} \Theta(n\Omega_{e} - \omega_{r})n^{2}\Omega_{e}^{2} \int_{0}^{x_{*}} dx \frac{x - x_{0}}{x\sqrt{x_{*}^{2} - x^{2}}}$$

$$\times \left(\frac{1}{\sqrt{2}x}\right) J_{n}^{2}(bx) \exp\left[-(x - x_{0})^{2} - \frac{\alpha_{\perp}^{2}}{\alpha_{\parallel}^{2}}(x_{*}^{2} - x^{2})\right]. \quad (12)$$

Here, the quantities x_0 , b, and x_* are defined exactly as in Eq. (5).

Before moving on, it is appropriate to make a little digression. We should note that while the purpose of the present choice of perpendicular ring electron distribution, $f_{\rm ring} \propto \exp{[-(v_{\perp}-v_0)^2/\alpha_{\perp}^2]}$, is to rectify the shortcoming of the DGH model, $f_{\rm DGH} \propto v_{\perp}^{2l} \exp{(-v_{\perp}^2/\alpha_{\perp}^2)}$, in that the integer l value is not flexible enough to model the time-dependence of both the thermal spread and the peak perpendicular velocity, it would also have been possible to resolve the issue by simply relaxing the integer l to a real value. Indeed, such a model is known as the chi-distribution, $f_{\mathrm{chi}}(v_{\perp}) = N v_{\perp}^{k-1} \exp{(-v_{\perp}^2/\alpha_{\perp}^2)}$, where k is a continuous parameter and the normalization constant is given by $N^{-1}=\pi\alpha^{k+1}\hat{\Gamma}[(k+1)/$ 2]—this follows from the requirement, $1 = 2\pi N \int_0^\infty dv_\perp v_\perp f_{\rm chi}(v_\perp)$. Obviously, k = 1 corresponds to the thermal distribution, and the choice of k = 2l + 1 leads to the DGH model. One could take the second and fourth velocity moments of the distribution, $\langle v_{\perp}^2 \rangle$ $= 2\pi \int_{0}^{\infty} dv_{\perp} v_{\perp}^{2} f_{\text{chi}}(v_{\perp}) = (k+3)\alpha_{\perp}^{2}/2$ and $\langle v_{\perp}^{4} \rangle = 2\pi \int_{0}^{\infty} dv_{\perp} v_{\perp}^{4}$ $\times f_{\text{chi}}(v_{\perp}) = (k+3)(k+5)\alpha_{\perp}^4/4$, from which we may extricate the evolution equations for α_{\perp} and k in the same manner as in Eq. (11). Obviously, this alternative choice (which was suggested by an anonymous reviewer) is beyond the scope of the present paper, but it is certainly possible to employ the chi distribution both in the PIC simulation and the reduced quasilinear analysis. However, such a task constitutes an entirely separate effort, and in the remainder of the present article, we return to the quasilinear analysis based upon the ring model.

Figure 6 displays the result of quasilinear analysis. The top panel plots the normalized ring speed, v_0/c , the middle panel corresponds to the thermal spread associated with the hot ring electrons, α_{\perp}/c , and the bottom panel shows the electrostatic wave energy density, $\int dk_{\perp}k_{\perp}W(k_{\perp})$, vs dimensionless time, Ω_{et} . We also indicate the time intervals, t=0 (the initial time), middle of the wave growth phase, which we choose to be $\Omega_e t=3.5$, quasi-saturation phase, which we designate as $\Omega_e t=10$, and the time at which the wave intensity undergoes a reduction, which we chose as $\Omega_e t=16$, and the final time $\Omega_e t=20$. These intervals are marked by vertical lines. Based on the instantaneous values of v_0 and α_{\perp} at these time periods, we may construct the instantaneous perpendicular velocity distribution function by substituting these values to the model equation (4), which will be shown later.

In Fig. 7, we plot the dynamic spectrum computed on the basis of present simplified quasilinear analysis. This result compares rather well with the simulated dynamic spectrum shown in Fig. 3. The narrow spectrum corresponds to the most unstable mode n=10 (see Fig. 1). At some later time, around $\Omega_e t=10$ or so, the next higher harmonic mode n=11 also begins to be generated. In the simulation, the spectrum surrounding the most intense region of wave numbers is somewhat broader than the quasilinear calculation, and the exact wave number corresponding to the peak wave growth is slightly less than $k\alpha_0/\Omega_e=1.5$, as noted already. In spite of such small discrepancies, the overall comparison is quite reasonable.

Finally, instantaneous perpendicular velocity distribution function is displayed in Fig. 8. The four time steps besides the initial state, $t\!=\!0$, namely, $\Omega_e t=3.5,\,\Omega_e t=10,\,\Omega_e t=16,$ and $\Omega_e t=20,$ which correspond to the wave growth period, quasi saturation stage, the stage when the wave intensity suffers gradual reduction, and the final computational time, are chosen. The snapshots of ring distribution at these intervals are reconstructed from the instantaneous values of v_0 and α_\perp at each time step. The overall profile of the perpendicular velocity distribution function at each time step is qualitatively similar to the

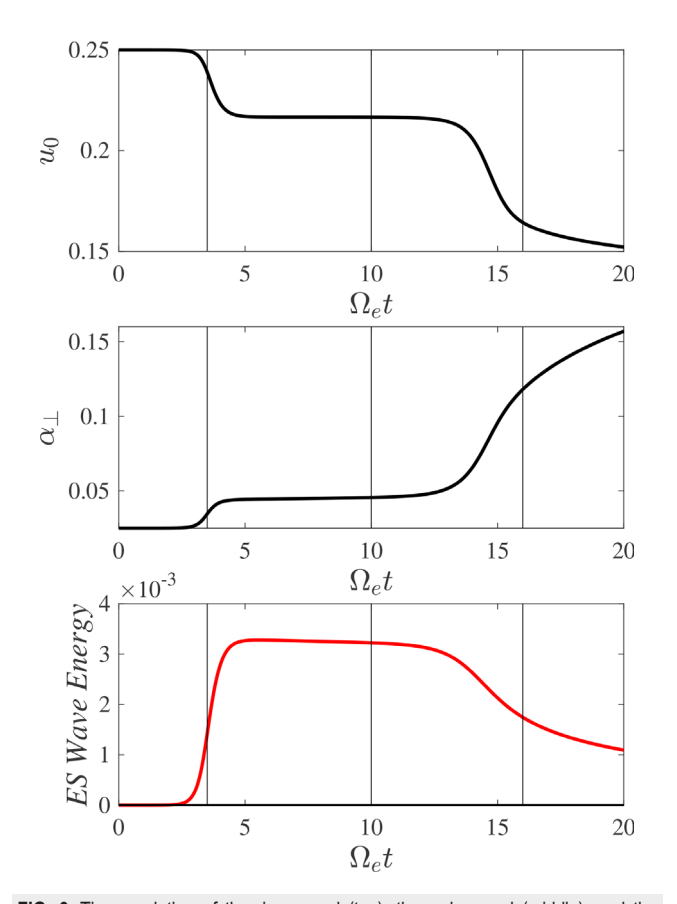


FIG. 6. Time evolution of the ring speed (top), thermal spread (middle), and the electrostatic wave energy density (bottom). Vertical lines mark the time intervals, which will be used to reconstruct the snapshots of velocity distribution functions.

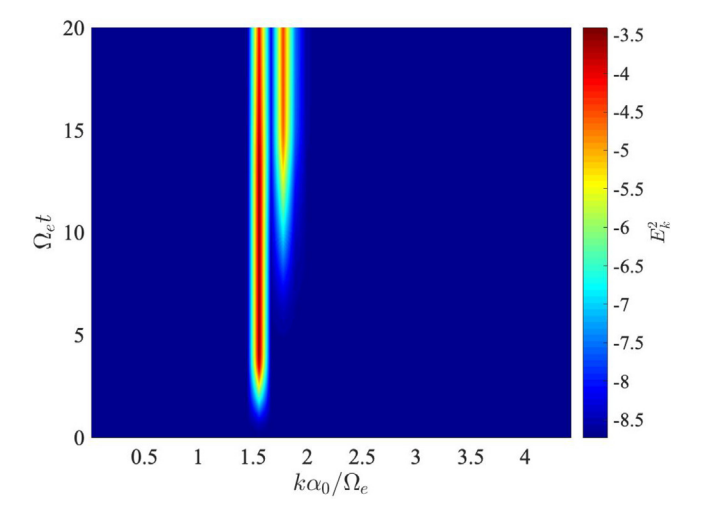


FIG. 7. Dynamic spectrum computed on the basis of reduced quasilinear theory.

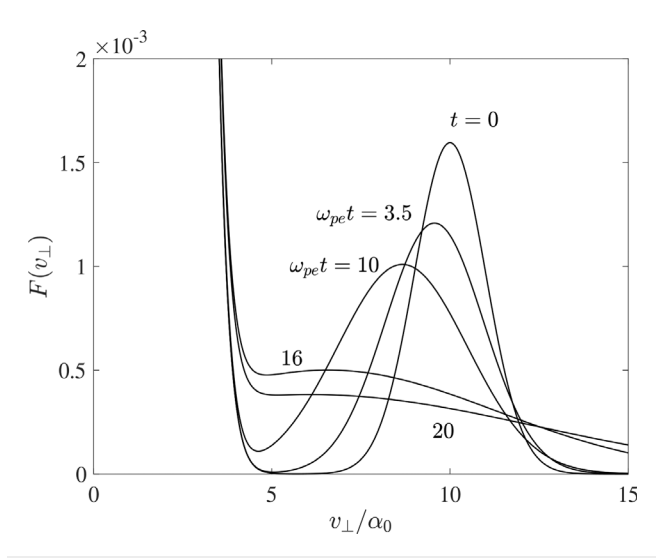


FIG. 8. Snapshot of perpendicular velocity distribution function constructed on the basis of instantaneous v_0 and α_\perp .

simulated electron distribution shown in Fig. 5. Although admittedly, the particle distribution computed from the simulation is not exactly the ring form, the overall sense of reduction in the ring speed and thermal spread along perpendicular velocity space are captured by the reduced quasilinear model. That the present reduced quasilinear theory is capable of reproducing the simulation result, at least in a qualitative sense despite the fact that the model electron distribution does not exactly describe the true time evolution of the velocity distribution, is in and of itself, quite remarkable. This finding points to the overall validity of the present methodology, which could have a wider ramification.

V. SUMMARY, CONCLUSION, AND DISCUSSION

In the present paper, we have carried out a comparative study of upper-hybrid instability driven by an initial ring electron distribution, by employing an approximate quasilinear analysis, guided by the PIC simulation. The type of quasilinear theory employed in the present study assumes that the particle distribution function can be modeled by an analytical time-dependent form. Such modeling must be done carefully to reflect the actual physics. In the context of solar wind research, the time-dependent bi-Maxwellian distribution has been quite successfully used for various temperature anisotropy-driven instabilities.^{54–63} The reason for such a success, especially if the excessive temperature anisotropy is in the perpendicular direction, is because the temperature anisotropy-driven instabilities are of the transverse type, for which the cyclotron resonance translates to the pitch-angle diffusion in velocity space. The end result is that the bi-Maxwellian nature of the underlying particle distribution is approximately preserved while the temperature anisotropy is being reduced. However, in the present case of an initial ring, or more generally, the loss-cone instability, the time evolution of the electron distribution is not trivial to predict a priori. In order to guide the theoretical modeling, we have, thus, first carried out a one-dimensional electrostatic (1D ES) particle-in-cell (PIC) code simulation. Guided by the results of simulation, we have subsequently modeled the time-dependent hot electron distribution by the same ring form, except that the ring speed

 v_0 and thermal spread α_\perp are allowed to vary in time. Upon verifying the result of such a reduced quasilinear theory against the PIC simulation, it is found that the quasilinear method quite reasonably reproduces the simulation result.

The significance of the present paper is that a similar type of quasilinear analysis may be extended to other types of plasma instabilities. As noted, this type of reduced quasilinear, sometimes called the velocity moment-based quasilinear theory (since one takes a finite number of velocity moments of the particle kinetic equation to extract the dynamic equations for time-dependent parameters), or macroscopic quasilinear theory (since the procedure of deriving the dynamic equations for the time-dependent parameters is analogous to formulating a macroscopic fluid theory from a kinetic equation), has thus far been quite extensively applied for the temperature anisotropy instabilities driven by bi-Maxwellian form of particle distributions. However, other types of plasma instabilities driven by different forms of particle distributions may also be treated with this type of analysis. The present ring electron distribution and upper-hybrid instability is one such example.

Before we close, we note that the present paper is largely motivated by quasi electrostatic fluctuations in the upper-hybrid frequency range pervasively detected in the terrestrial or planetary magnetosphere, which is presumably excited by the electron ring distribution, which is a form of loss-cone. However, the occurrence of ring or non gyrotropic ring (also known as the agyrotropic crescent) electron distribution can take place in other physical situations. For instance, such a distribution of electrons have been seen in numerical simulations of magnetic reconnection exhausts, e.g., Refs. 65 and 66. Such electron distributions are detected by Magnetospheric Multi-Scale (MMS) spacecraft close to the electron diffusion region, which are accompanied by intense high-frequency upper-hybrid fluctuations. This broadens the relevance of the present methodology to situations beyond the magnetospheric applications.

ACKNOWLEDGMENTS

P.H.Y. acknowledges NSF under Grant No. 2203321 and NASA under Grant No. 80NSSC23K0662 to the University of Maryland. This material was based upon work funded by the Department of Energy (No. DE-SC0022963) through the NSF/DOE Partnership in Basic Plasma Science and Engineering. P.H.Y. also acknowledges the hospitality of Kyoto University, Japan, for hosting his visit during the time period over which the present research was carried out. Y.O. was supported by JSPS KAKENHI under Grant No. JP20H01960.

AUTHOR DECLARATIONS Conflict of Interest

The authors have no conflicts to disclose.

Author Contributions

Peter H. Yoon: Conceptualization (equal); Formal analysis (equal); Investigation (equal); Methodology (equal); Software (equal); Validation (equal); Visualization (equal); Writing – original draft (equal); Writing – review & editing (equal). **Yoshiharu Omura:** Formal analysis (equal); Investigation (equal); Methodology (equal); Resources (equal); Software (equal); Validation (equal); Visualization (equal); Writing – review & editing (equal).

DATA AVAILABILITY

Data sharing is not applicable to this article as no new data were created or analyzed in this study.

REFERENCES

- ¹P. Christiansen, P. Gough, G. Martelli, J.-J. Bloch, N. Cornilleau, J. Etcheto, R. Gendrin, D. Jones, C. Béghin, and P. Décréau, Nature 272, 682 (1978).
- ²P. J. Christiansen *et al.* "GEOS-1 observations of electrostatic waves, and their relationship with plasma parameters," in *Advances in Magnetosperic Physics with GEOS-1 and ISEE*, edited by K. Knott, A. Durney, and K. Ogilvie (Springer, Dordrecht, 1978).
- ³W. S. Kurth, J. D. Craven, L. A. Frank, and D. A. Gurnett, J. Geophys. Res. **84**, 4145, https://doi.org/10.1029/JA084iA08p04145 (1979).
- ⁴W. S. Kurth, M. Ashour-Abdalla, L. A. Frank, C. F. Kennel, D. A. Gurnett, D. D. Sentman, and B. G. Burek, Geophys. Res. Lett. **6**, 487, https://doi.org/10.1029/GL006i006p00487 (1979).
- ⁵P. C. Filbert and P. J. Kellogg, J. Geophys. Res. **84**, 1369–1381, https://doi.org/ 10.1029/JA084iA04p01369 (1979).
- ⁶H. Matsumoto and H. Usui, Geophys. Res. Lett. 24, 49, https://doi.org/ 10.1029/96GL03650 (1997).
- ⁷H. Usui, W. R. Paterson, H. Matsumoto, L. A. Frank, M. Nakamura, H. Matsui, T. Yamamoto, O. Nishimura, and J. Koizumi, J. Geophys. Res. 104, 4477, https://doi.org/10.1029/1998JA900151 (1999).
- ⁸W. S. Kurth, S. De Pascuale, J. B. Faden, C. A. Kletzing, G. B. Hospodarsky, S. Thaller, and J. R. Wygant, J. Geophys. Res. 120, 904, https://doi.org/10.1002/2014JA020857 (2015).
- ⁹I. B. Bernstein, Phys. Rev. **109**, 10 (1958).
- ¹⁰F. W. Crawford, Radio Sci. J. Res. **69**(6), 789–805 (1965).
- ¹¹F. W. Crawford and J. A. Tataronis, J. Appl. Phys. **36**, 2930–2934 (1965).
- ¹²F. W. Crawford, R. S. Harp, and T. D. Mantei, J. Geophys. Res. 72, 57, https://doi.org/10.1029/JZ072i001p00057 (1967).
- ¹³R. W. Fredericks, J. Geophys. Res. **76**, 5344, https://doi.org/10.1029/ JA076i022p05344 (1971).
- ¹⁴T. S. Young, J. D. Callen, and J. E. McCune, J. Geophys. Res. 78, 1082, https://doi.org/10.1029/JA078i007p01082 (1973).
- ¹⁵V. I. Karpman, J. K. Alekhin, N. D. Borisov, and N. A. Rjabova, Plasma Phys. 17, 361 (1975).
- ¹⁶V. V. Zheleznyakov and E. Y. Zlotnik, Sol. Phys. **43**, 431 (1975).
- ¹⁷M. Ashour-Abdalla and C. F. Kennel, J. Geophys. Res. 83(4), 1531–1534, https://doi.org/10.1029/JA083iA04p01531 (1978).
- ¹⁸R. F. Hubbard and T. J. Birmingham, J. Geophys. Res. 83, 4837, https://doi.org/ 10.1029/JA083iA10p04837 (1978).
- ¹⁹G. D. Fleishman and G. Yastrebov, Sol. Phys. **154**, 361 (1994).
- ²⁰P. H. Yoon and C. S. Wu, J. Geophys. Res. **104**, 19801, https://doi.org/10.1029/1999JA900253 (1999).
- ²¹D. D. Sentman, J. Geophys. Res. 87, 1455, https://doi.org/10.1029/ JA087iA03p01455 (1982).
- ²²N. Meyer-Vernet, S. Hoang, and M. Moncuquet, J. Geophys. Res. **98**, 21163, https://doi.org/10.1029/93JA02587 (1993).
- ²³K. Issautier, M. Moncuquet, N. Meyer-Vernet, S. Hoang, and R. Manning, Astrophys. Space Sci. 277, 309 (2001).
- ²⁴M. Moncuquet, A. Lecacheux, N. Meyer-Vernet, B. Cecconi, and W. S. Kurth, Geophys. Res. Lett. **32**, L20S02, https://doi.org/10.1029/2005GL022508 (2005).
- ²⁵P. H. Yoon, S. Kim, J. Hwang, and D.-K. Shin, J. Geophys. Res. **122**, 5365, https://doi.org/10.1002/2016JA023321 (2017).
- ²⁶J. Hwang, D. K. Shin, P. H. Yoon, W. S. Kurth, B. A. Larsen, G. D. Reeves, and D. Y. Lee, Phys. Plasmas 24, 062904 (2017).
- ²⁷P. H. Yoon and R. A. López, Phys. Plasmas **24**, 022117 (2017).
- ²⁸R. A. López and P. H. Yoon, Plasmas Phys. Controlled Fusion 59, 115003 (2017).
- ²⁹S. Kim, R. Schlickeiser, P. H. Yoon, R. A. López, and M. Lazar, Plasmas Phys. Controlled Fusion 59, 125003 (2017).
- ³⁰J. Hwang and P. H. Yoon, J. Geophys. Res. 123, 9239–9251, https://doi.org/ 10.1029/2018JA025643 (2018).

- ³¹P. H. Yoon, J. Hwang, H. Kim, and J. Seough, J. Geophys. Res. 124, 2811–2818, https://doi.org/10.1029/2019JA026460 (2019).
- 32 E. G. Harris, Phys. Rev. Lett. 2, 34 (1959).
- ³³E. G. Harris, J. Nucl. Energy, Part C 2, 138 (1961).
- 34G. Bekefi, J. D. Coccoli, E. B. Hooper, Jr., and S. J. Buchsbaum, Phys. Rev. Lett. 9, 6 (1962)
- ³⁵R. A. Dory, G. E. Guest, and E. G. Harris, *Phys. Rev. Lett.* **14**, 131 (1965).
- ³⁶J. E. Allen and A. D. R. Phelps, Rep. Prog. Phys. **40**, 1305 (1977)
- ³⁷D. G. Lominadze, *Cyclotron Waves in Plasmas* (Pergamon, Oxford, 1981).
- ³⁸P. H. Yoon, F. Hadi, and A. Qamar, *Phys. Plasmas* **21**, 074502 (2014).
- ³⁹J. M. Dawson, Phys. Fluids **13**, 1819 (1970).
- 40 T. Kamimura, T. Wagner, and J. M. Dawson, Phys. Fluids 21, 1151 (1978).
- ⁴¹M. Ashour-Abdalla, J. N. Leboeuf, J. M. Dawson, and C. F. Kennel, Geophys. Res. Lett. 7, 889, https://doi.org/10.1029/GL007i011p00889 (1980).
- ⁴²J. M. Dawson, Phys. Scr. T2 1, 20 (1982).
- ⁴³J. M. Dawson, Rev. Mod. Phys. **55**, 403 (1983).
- ⁴⁴T. Umeda, M. Ashour-Abdalla, D. Schriver, R. L. Richard, and F. V. Coroniti, J. Geophys. Res. 112, A04212, https://doi.org/10.1029/2006JA012124 (2007).
- ⁴⁵B. Eliasson, D. C. Speirs, and L. K. S. Daldorff, Plasma Phys. Controlled Fusion 58, 095002 (2016).
- ⁴⁶B. Eliasson, M. Viktorov, D. C. Speirs, K. Ronald, D. Mansfeld, and A. D. R. Phelps, Phys. Rev. Res. 2, 043272 (2020).
- ⁴⁷M. Horký, Y. Omura, and O. Santolik, Phys. Plasma 25, 042905 (2018).
- ⁴⁸M. Horký and Y. Omura, Phys. Plasma **26**, 022904 (2019).
- 49 X. Zhou, P. A. Muñoz, J. Büchner, and S. Liu, Astrophys. J. 891, 92 (2020).
- ⁵⁰A. Tarasov, A. Shagayda, I. Khmelevskoi, D. Kravchenko, and A. Lovtsov, Phys. Plasmas 28, 102108 (2021).
- ⁵¹A. I. Akhiezer, I. A. Akhiezer, R. V. Polovin, A. G. Sitenko, and K. N. Stepanov, Electrodynamics of Plasma (Nauka, Moscow, 1974) (in Russian).
- 52S. M. Grach, Radiophys. Quantum Electron. 42, 572–588 (1999).
- ⁵³J. Lee, P. H. Yoon, J. Seough, R. A. López, J. Hwang, J. Lee, and G. S. Choe, J. Geophys. Res. **123**, 7230–7331 (2018).
- ⁵⁴S.-Y. Lee, E. Lee, J. Seough, J.-G. Lee, J. Hwang, J.-J. Lee, K.-S. Cho, and P. H. Yoon, J. Geophys. Res. 123, 3277, https://doi.org/10.1029/2017JA024960 (2018).
- ⁵⁵J. Seough, P. H. Yoon, and J. Hwang, Phys. Plasmas **21**, 062118 (2014).
- ⁵⁶J. Seough, P. H. Yoon, and J. Hwang, Phys. Plasmas **22**, 012303 (2015).
- 57 J. Seough, P. H. Yoon, J. Hwang, and Y. Nariuki, Phys. Plasmas 22, 082122 (2015).
- ⁵⁸A. Stockem-Novo, P. H. Yoon, M. Lazar, R. Schlickeiser, S. Poedts, and J. Seough, Phys. Plasmas 22, 092301 (2015).
- ⁵⁹P. H. Yoon, J. Seough, and Y. Nariyuki, J. Geophys. Res. **120**, 6071, https://doi.org/10.1002/2015JA021495 (2015).
- ⁶⁰P. H. Yoon, R. A. López, J. Seough, and M. Sarfraz, Phys. Plasmas 24, 112104 (2017)
- ⁶¹H. P. Kim, J. Seough, J. Hwang, and P. H. Yoon, J. Geophys. Res. 122, 4410–4419, https://doi.org/10.1002/2016JA023558 (2017).
- ⁶²P. H. Yoon, J. Lee, J. Hwang, J. Seough, and G. S. Choe, J. Geophys. Res. **124**, 5289–5301, https://doi.org/10.1029/2019JA026687 (2019).
- 63 M. Sarfraz, R. A. López, S. Ahmed, and P. H. Yoon, Mon. N. R. Astron. Soc.
- 509, 3764-3771 (2021).

 64Y. Omura and H. Matsumoto, "Kempo1: Technical guide to one dimensional electromagnetic particle code" in Computer Space Plasma Physics: Simulation
- electromagnetic particle code," in *Computer Space Plasma Physics: Simulation Techniques and Software*, edited by H. Matsumoto and Y. Omura (Terra Sci., Tokyo, 1993), pp. 21–65.
- ⁶⁵J. R. Shuster, L.-J. Chen, W. S. Daughton, L. C. Lee, K. H. Lee, N. Bessho, R. B. Torbert, G. Li, and M. R. Argail, Geophys. Res. Lett. 41, 5389–5395, https://doi.org/10.1002/2014GL060608 (2014).
- ⁶⁶M. H. Barbhuiya, P. A. Cassak, M. A. Shay, V. Roystershteyn, M. Swisdak, A. Caspi, A. Runov, and H. Liang, J. Geophys. Res. 127, e2022JA030610 (2022).
- ⁶⁷J. L. Burch, K. Dokgo, K. J. Hwang, R. B. Torbert, D. B. Graham, J. M. Webster, R. E. Ergun, B. L. Giles, R. C. Allen, L.-J. Chen, S. Wang, K. J. Genestreti, C. T. Russell, R. J. Strangeway, and O. Le Contel, Geophys. Res. Lett. 46, 4089–4097, https://doi.org/10.1029/2019GL082471 (2019).
- 68 K. Dokgo, K.-J. Hwang, J. L. Burch, E. Choi, P. H. Yoon, D. G. Sibek, and D. B. Graham, Geophys. Res. Lett. 46, 7873–7882, https://doi.org/10.1029/2019GL083361 (2019)